

rspa.royalsocietypublishing.org

N. J. Balmforth¹, R. V. Craster² and I. J. Hewitt³

Research



Cite this article: Balmforth NJ, Craster RV, Hewitt IJ. 2015 The speed of an inclined ruck. *Proc. R. Soc. A* **471**: 20140740. <http://dx.doi.org/10.1098/rspa.2014.0740>

Received: 30 September 2014

Accepted: 14 November 2014

Subject Areas:

applied mathematics, mechanical engineering

Keywords:

elastic beam, adhesion, peeling

Author for correspondence:

R. V. Craster

e-mail: r.craster@imperial.ac.uk

¹Department of Mathematics, University of British Columbia, 1984 Mathematics Road, Vancouver, British Columbia, Canada V6T 1Z2

²Department of Mathematics, Imperial College London, South Kensington Campus, London SW7 2AZ, UK

³Mathematical Institute, University of Oxford, Oxford OX2 6GG, UK

Steady rucks in an elastic beam can roll at constant speed down an inclined plane. We examine the dynamics of these travelling-wave structures and argue that their speed can be dictated by a combination of the physical conditions arising in the vicinity of the ‘contact points’ where the beam is peeled off the underlying plane and stuck back down. We provide three detailed models for the contact dynamics: viscoelastic fracture, a thermodynamic model for bond formation and detachment and adhesion mediated by a thin liquid film. The results are compared with experiments.

1. Introduction

Two recent articles, Kolinski *et al.* [1] and Vella *et al.* [2], have explored the dynamics of rucks propagating along elastic sheets in contact with an underlying plane. The dynamics of such structures has analogies with the mechanics of sliding crystal dislocations, earthquake slip pulses, Schallamach waves in rubber and bio-locomotion strategies exploiting contact (e.g. [3–7]). Kolinski *et al.* [1], in particular, explored experimentally the shapes and speeds of rucks driven forwards by a body force such as gravity, by emplacing the elastic sheet on an inclined plane.

To achieve steadily moving rucks, the potential energy released by rolling must be dissipated. Kolinski *et al.* [1] argue that air resistance is primarily responsible, although their scaling theory predicts that rolling speeds should decrease with ruck amplitude, in stark contrast with experimental observations. These authors also briefly consider, and dismiss, visco-elastic losses in the bulk of the deforming sheet. They report the further interesting observations that a threshold tilt of the plane

is required for rucks to begin rolling, and that once the ruck is in motion, a lower tilt angle is required to arrest that rolling.

Here, we revisit this problem, exploring in more detail what might set the speed of a rolling ruck. We offer a brief recapitulation of the analysis of Kolinski *et al.*, which corrects a detail of their scaling theory. The main premise of our study, however, is that it is the detailed peeling dynamics near the contact points at the edges of the ruck that dictates the speed. This is in analogy with the rolling friction of a cylinder or sphere on an elastic substrate (e.g. [8,9]) and a number of other fluid mechanical ‘peeling’ problems (e.g. [10,11]). It demands consideration of a local ‘microscopic’ model for the two peeling regions, which constitutes the bulk of our analysis.

We consider three possible peeling models in particular: viscoelastic dissipation at a fracture (which is commonly used in the solid mechanics literature for delamination or adhesion of elastomers to a substrate; (e.g. [12,13])), a thermodynamic model based on the kinetics of interfacial bonds bridged between the surfaces [14], and adhesion by a viscous fluid film (the McEwan–Taylor peeling problem; [15]). All three of these models are motivated by work on elastomer adhesion where viscoelastic losses, interfacial bonds and liquid coatings are all inferred to contribute (e.g. [16–18]). Our main goal is to determine whether such peeling models can describe the parametric dependence of ruck rolling speeds and the threshold for motion. We close by comparing the theory with a series of experiments and with the older results of Kolinski *et al.* [1].

2. Ruck dynamics

(a) Mathematical formulation

Consider an elastic plate of undeformed thickness d and density ρ resting on an inclined rigid plane; θ is the angle of inclination. The uphill edge of the plate is brought downwards a distance \mathcal{E} along the plane to form a localized ruck, as sketched in figure 1. Assuming everything remains two-dimensional, we describe the position of the plate in terms of arc length s at time t : $(X(s, t), Z(s, t))$. Denoting the local stress resultant by (N_X, N_Z) , the equations of motion of the ruck, where it is lifted off the plane, are [1,19]

$$\left. \begin{aligned} \frac{\partial}{\partial s} N_X + \rho g d \sin \theta &= \rho d \frac{\partial^2 X}{\partial t^2}, \\ \frac{\partial}{\partial s} N_Z - \rho g d \cos \theta &= \rho d \frac{\partial^2 Z}{\partial t^2} \end{aligned} \right\} \quad (2.1)$$

and
$$\frac{\partial M}{\partial s} - N_X \sin \phi + N_Z \cos \phi = 0,$$

where $\phi(s, t)$ is the local angle that the centerline of the plate makes with the x -axis; g is the gravitational acceleration and M is the local bending moment. The geometry dictates

$$\frac{\partial X}{\partial s} = \cos \phi, \quad \frac{\partial Z}{\partial s} = \sin \phi \quad \text{and} \quad \kappa = \frac{\partial \phi}{\partial s}, \quad (2.2)$$

where κ is the local curvature. The moment and curvature are related by $M = B\kappa$, where B is the bending stiffness. For locations where the plate is in contact with the plane, we assume that the normal reaction and friction are always sufficient to hold it in place with $Z = 0$ (cf. [2]).

We locate the edges of the ruck at $s = s_{\pm}(t)$. Here,

$$X(s_{\pm}, t) = \begin{cases} s_{-}(t) + \mathcal{E}, & Z(s_{\pm}, t) = 0, \quad \phi(s_{\pm}, t) = 0, \\ s_{+}(t), & \end{cases} \quad (2.3)$$

(the plate is shifted downhill by \mathcal{E} for $s \leq s_{-}$ and is not displaced for $s \geq s_{+}$). The final condition reflects our assumption that bending is sufficiently important in the vicinity of the contact points that the plate meets the plane tangentially; we reserve judgement on the local curvatures,

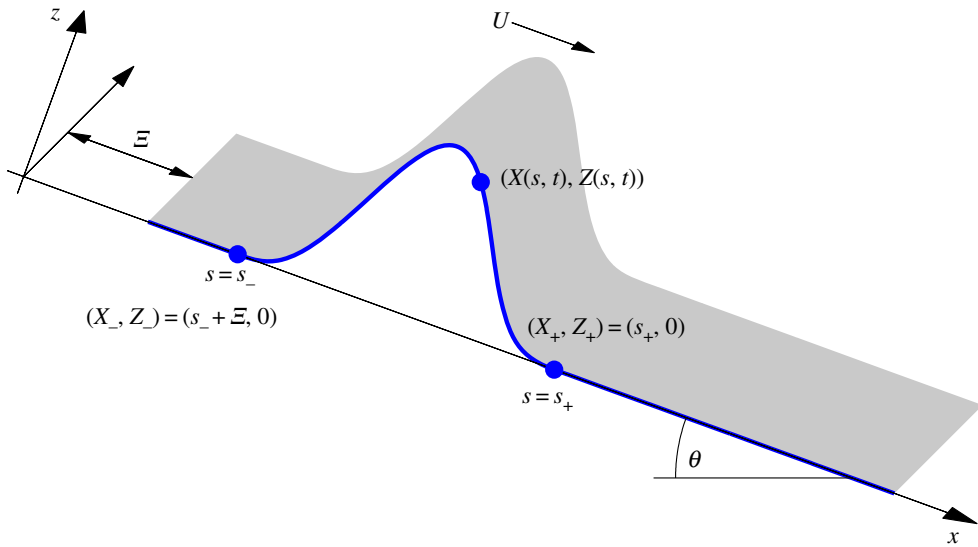


Figure 1. Sketch of a ruck rolling with speed U , showing the imposed foreshortening \mathcal{E} , the angle of the inclined plane θ and the two-dimensional ruck shape $(X(s, t), Z(s, t))$, where s is the arc length and the ruck occupies $s_- < s < s_+$. (Online version in colour.)

$\kappa_{\pm} = \kappa(s_{\pm}, t)$, until later. Note that (2.2) in combination with the total time derivative of quantities such as $\phi(s_{\pm}(t), t)$, imply

$$\phi_t(s_{\pm}, t) = -\kappa_{\pm} \dot{s}_{\pm}, \quad X_s(s_{\pm}, t) = 1 \quad \text{and} \quad X_t(s_{\pm}, t) = Z_s(s_{\pm}, t) = Z_t(s_{\pm}, t) = 0, \quad (2.4)$$

using (lower case) subscripts as shorthand for derivatives.

(b) Energetics

By multiplying (2.1a) by X_t , (2.1b) by Z_t and (2.1c) by ϕ_t , then integrating in s , one can derive the energy equation

$$\frac{d}{dt} \int_{s_-}^{s_+} \mathcal{E} ds = [\mathcal{E}\dot{s} + M\phi_t]_{s_-}^{s_+}, \quad (2.5)$$

where

$$\mathcal{E} = \frac{1}{2} \rho d (X_t^2 + Z_t^2) + \frac{1}{2} B \kappa^2 + \rho g d (Z \cos \theta - X \sin \theta) \quad (2.6)$$

is the energy density and \dot{s} represents \dot{s}_{\pm} . The power input on the right-hand side of (2.5) contains the energy flux owing to the motion of the contact points ($\mathcal{E}\dot{s}$) and the work done by the local moment ($M\phi_t$).

For steady rolling at speed U , $\dot{s}_{\pm} \equiv U$, and

$$[M\phi_t]_{s_-}^{s_+} = -BU(\kappa_+^2 - \kappa_-^2), \quad [\mathcal{E}\dot{s}]_{s_-}^{s_+} = \frac{1}{2}BU(\kappa_+^2 - \kappa_-^2) - \rho g d U(s_+ - s_- - \mathcal{E}) \sin \theta,$$

and hence evaluating (2.5) yields

$$\frac{d}{dt} \int_{s_-}^{s_+} \mathcal{E} ds = -\frac{1}{2}BU(\kappa_+^2 - \kappa_-^2) - \rho g d U(s_+ - s_- - \mathcal{E}) \sin \theta. \quad (2.7)$$

For steady rolling, this rate of change of ruck energy must equal the rate of change of potential energy owing to translation along the plane, i.e.

$$\frac{d}{dt} \int_{s_-}^{s_+} \mathcal{E} ds = -\rho g d (s_+ - s_-) U \sin \theta. \quad (2.8)$$

Equating (2.8) and (2.5) then gives the relationship

$$\frac{1}{2}B(\kappa_+^2 - \kappa_-^2) = \rho g d \mathcal{E} \sin \theta. \quad (2.9)$$

The right-hand side of (2.9) is the potential energy released by rolling; the left is the bending energy required to peel off (and lay down) the plate from the plane at the contact points. By analogy with fracture mechanics, we demand that the latter is equal to the effective work of adhesion, w .

In §4, we determine w by considering the detailed mechanics of how contact and adhesion is actually achieved in three different models. We write the result formally in terms of functions $\mathcal{W}_\pm(U)$ that are yet to be defined

$$\frac{1}{2}B\kappa_\pm^2 = \mathcal{W}_\pm(U), \quad (2.10)$$

so that (2.9) becomes

$$\mathcal{W}_+(U) - \mathcal{W}_-(U) = \rho g d \mathcal{E} \sin \theta. \quad (2.11)$$

Importantly, if one discards inertia as we do below, the ruck speed U appears only in these peeling conditions. In other words, the overall shape of the structure reflects a quasi-static force balance and peeling dictates the ruck speed.

Note that (2.9) also applies for static rucks (one multiplies the steady versions of (2.1) by $(\cos \phi, \sin \phi, \kappa)$, integrates in s and uses the boundary conditions and $\int_{s_-}^{s_+} (X_s, Z_s) ds = \int_{s_-}^{s_+} (\cos \phi, \sin \phi) ds = (s_+ - s_- \mathcal{E}, 0)$), immobilized either by the action of an external force or because the energy released by rolling is not sufficient to overcome the energy of adhesion. For the latter, this would require

$$\rho g d \mathcal{E} \sin \theta < \mathcal{W}_+(0) - \mathcal{W}_-(0). \quad (2.12)$$

(c) Ruck shapes

Assuming that ruck rolling is relatively slow, we now ignore inertia. Because there are no longer any time derivatives in the ruck equations, we can then consider the moving frame in which the contact points are stationary and located at $s=0$ and $s=L$, where L is the total arc length of the ruck. This length is actually not known, but must be determined as part of the solution of the problem once the foreshortening length \mathcal{E} and tilt angle θ are prescribed.

Although there is a natural bending-gravity length scale given by

$$L_b = \left(\frac{B}{\rho g d} \right)^{1/3}, \quad (2.13)$$

we use L to measure lengths so that the spatial domain becomes fixed. We then set

$$s = L\hat{s}, \quad (X, Z) = L(\hat{X}, \hat{Z}), \quad (N_X, N_Z) = \frac{B}{L^2}(\hat{N}_X, \hat{N}_Z) \quad \text{and} \quad \kappa = \frac{1}{L}\hat{\kappa}, \quad (2.14)$$

to recast the model in the dimensionless form

$$\frac{\partial \hat{X}}{\partial \hat{s}} = \cos \phi, \quad \frac{\partial \hat{Z}}{\partial \hat{s}} = \sin \phi \quad \text{and} \quad \hat{\kappa} = \frac{\partial \phi}{\partial \hat{s}}, \quad (2.15)$$

$$\frac{\partial \hat{N}_X}{\partial \hat{s}} + \ell^3 \sin \theta = 0 \quad \text{and} \quad \frac{\partial \hat{N}_Z}{\partial \hat{s}} - \ell^3 \cos \theta = 0 \quad (2.16)$$

$$\text{and} \quad \frac{\partial \hat{\kappa}}{\partial \hat{s}} - \hat{N}_X \sin \phi + \hat{N}_Z \cos \phi = 0, \quad (2.17)$$

with boundary conditions

$$\phi(0) = \phi(1) = \hat{Z}(0) = \hat{Z}(1) = \hat{X}(0) = 0 \quad \text{and} \quad \hat{X}(1) = 1 - \frac{\chi}{\ell}, \quad (2.18)$$

where

$$\chi = \frac{\mathcal{E}}{L_b} \quad \text{and} \quad \ell = \frac{L}{L_b}. \quad (2.19)$$

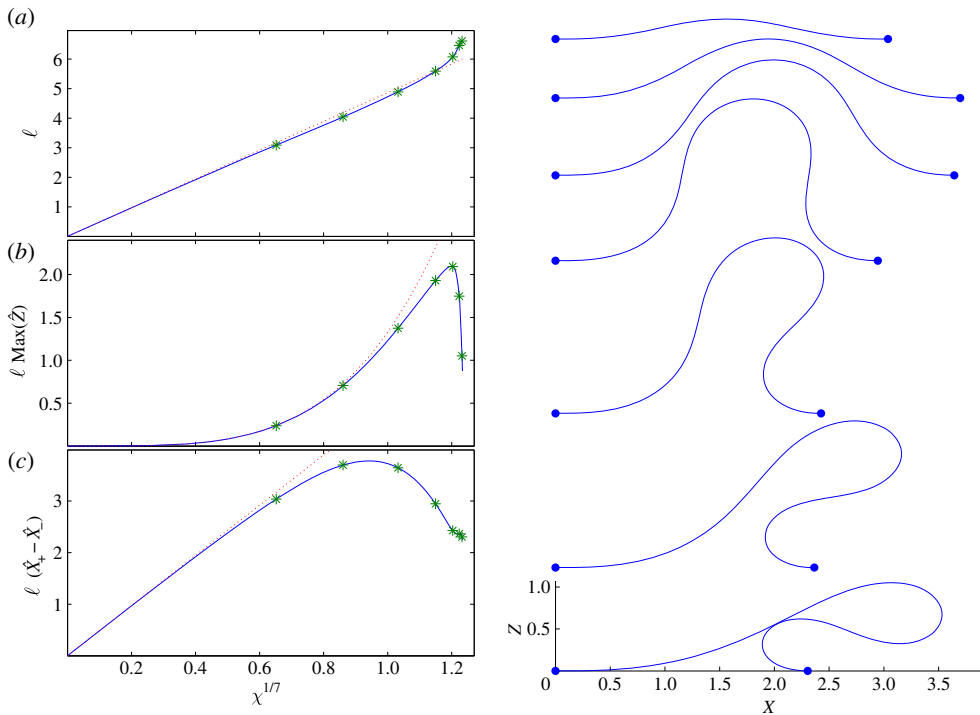


Figure 2. Sample numerical solutions for steadily rolling rucks with $\phi_s(0) = \hat{\kappa}_- = 0$, $\theta = 10^\circ$ and varying χ . Shown are (a) ruck arc length ℓ , (b) ruck height $\ell \text{Max}(\hat{Z})$ and (c) the distance between the contact points, $\ell(\hat{X}_+ - \hat{X}_-)$, all plotted against $\chi^{1/7}$. The dotted lines show the low-amplitude predictions from (2.24). The stars indicate the solutions whose profiles are plotted on the right. (Online version in colour.)

Specification of the peeling conditions,

$$\hat{\kappa}_\pm = \ell \left[\frac{2L_b^2 \mathcal{W}_\pm(U)}{B} \right]^{1/2}, \quad (2.20)$$

provides two further constraints to determine the ruck speed U and length ℓ .

Given the integral constraint (2.11), we may divorce the problems of finding the ruck speed, and its shape and length. For a given \mathcal{E} and θ , (2.11) determines the speed, while (2.15)–(2.19) may be supplemented with a prescription of one of the edge curvatures κ_\pm from (2.20) to form an ‘eigenvalue’ problem for the length ℓ and the ruck shape (the other edge curvature is then automatically satisfied through the integral condition (2.9)).

Sample numerical solutions to (2.15)–(2.18) with $\phi_s(0) = \kappa_- = 0$ are shown in figure 2. This choice for the uphill curvature corresponds to a situation in which the plate is gently laid back down on the plane without any interaction between the two surfaces. The ruck amplitude, $\ell \text{Max}(\hat{Z})$, grows with the foreshortening parameter χ until it reaches a maximum corresponding to the tallest ruck that can support itself against gravity; for larger foreshortenings, the ruck begins to topple downhill. Eventually, the toppling over terminates the solution at a self intersection (cf. [19,20]). During this sequence, the ruck total arc length ℓ increases steadily with χ , but the distance between the contact points on the plane, $\ell(\hat{X}_+ - \hat{X}_-)$, varies non-monotonically.

For low amplitudes, $\chi \ll 1$, one can find the ruck shapes analytically: in this limit, the solution has the scalings (cf. [2,19])

$$\phi \sim \chi^{3/7}, \quad \ell \sim \chi^{1/7}, \quad \hat{N}_X \sim -m^2 \quad \text{and} \quad \hat{N}_Z \equiv \hat{N}_Z(0) + \hat{s}\ell^3 \cos \theta \sim \chi^{3/7}, \quad (2.21)$$

where the order-one constant m and the small constant $\hat{N}_Z(0)$ are to be determined. Hence, to leading order

$$\phi_{\hat{s}\hat{s}} + m^2\phi + \hat{N}_Z(0) + \hat{s}\ell^3 \cos\theta = 0, \quad (2.22)$$

subject to

$$\phi(0) = \phi(1) = \phi_{\hat{s}}(0) = \int_0^1 \phi \, d\hat{s} = 0 \quad \text{and} \quad \int_0^1 \phi^2 \, d\hat{s} = \frac{2\chi}{\ell}. \quad (2.23)$$

The solution is

$$\phi \sim \frac{\ell^3 \cos\theta}{m^3} \left[\sin(m\hat{s}) - m\hat{s} + \frac{1}{2}m - \frac{1}{2}m \cos(m\hat{s}) \right] \quad \text{and} \quad \ell \sim \left(\frac{48 m^4 \chi}{5 \cos^2\theta} \right)^{1/7}, \quad (2.24)$$

where $m \approx 8.987$ is the solution to $\tan(\frac{1}{2}m) = \frac{1}{2}m$ and $\hat{N}_Z(0) = -\frac{1}{2}\ell^3 \cos\theta$.

3. Bulk dissipation

In the absence of adhesion, we have $\mathcal{W}_{\pm} = 0$ in (2.9), so another mechanism is needed to balance the potential energy release rate on the right-hand side, and hence set the motion of the ruck. Kolinski *et al.* [1] propose that either air resistance or bulk viscoelasticity in the plate could provide the required dissipation. The inclusion of either effect leads to additional terms in the energy balance (2.9). For instance, a viscoelastic rheology may be described most simply using the constitutive relation $M = B\kappa + C\kappa_t$, where C is the product of plate viscosity and moment of inertia [1]. In that case (2.9) becomes

$$\left[\frac{1}{2}B\kappa^2 + C\kappa\kappa_t \right]_{s_-}^{s_+} + \frac{C}{U} \int_{s_-}^{s_+} \kappa_t^2 \, ds = \rho g d \mathcal{E} \sin\theta. \quad (3.1)$$

The viscoelastic integral term on the left requires knowledge of the ruck shape to evaluate exactly, but can be estimated on dimensional grounds. In particular, $\kappa \sim \text{Max}(Z)/L^2$, and time scales as L/U , so the integral is of order $CUL^{-5}[\text{Max}(Z)]^2$. For a small ruck (see §2c), we have $L \sim \mathcal{E}^{1/7}$ and $\text{Max}(Z) \sim \mathcal{E}^{4/7}$, so this quantity scales as $U\mathcal{E}^{3/7}$. Assuming that this bulk viscoelastic term controls the dissipation, it can be compared with the potential energy release rate $\rho g d \mathcal{E} \sin\theta$, to extract the scaling $U \sim \mathcal{E}^{4/7} \sin\theta$. Similarly, one can estimate that air drag provides an energy loss rate of the order $\rho_{\text{air}}U^2\text{Max}(Z)$ and therefore suggests $U \sim \mathcal{E}^{3/14}(\sin\theta)^{1/2}$. Both of these mechanisms imply a rapid increase in speed with foreshortening; in neither case is there a threshold for rolling.

A similar scaling approach was also taken by Kolinski *et al.* [1]. Unfortunately, these authors used a different expression for the potential energy release rate, featuring the length of the ruck instead of the foreshortening \mathcal{E} . The effect is to furnish erroneous scalings $U \sim \mathcal{E}^{-2/7}$ and $U \sim \mathcal{E}^{-3/14}$ (for viscoelasticity and air drag, respectively), which suggest that the ruck speed should decrease with larger ruck amplitude. The correct scalings no longer have this counterintuitive property. Nevertheless, rough estimates of the material parameters suitable for our experiments (see §5 and appendix A), suggest ruck speeds of order 20 m s^{-1} according to the scalings for the two bulk dissipations. Our rucks, however, roll at speeds of centimetres per second. The ruck speed is also observed to increase more gradually with \mathcal{E} .

4. Peeling models

(a) Viscoelastic fracture

The peeling of adhering surfaces in solid mechanics is often identified as a problem of crack propagation. In this context, it is conventional to balance the energy released at the point of fracture with the work of adhesion w (e.g. [12,13]). For many problems involving the peeling of elastomers, the work of adhesion in opening the crack, w_{open} , is observed to depend on the (constant) speed at which the fracture propagates through the empirical relation (e.g. [9,18,21]),

$$w_{\text{open}} = w_0[1 + \varphi(a_T U)], \quad (4.1)$$

where w_0 is the adhesion energy at zero speed and a_T is a temperature-dependent factor dictated by the viscoelastic modulus of the material. The empirical function $\varphi(a_T U)$ is often presented as a power law $\varphi \sim U^n$ with exponent $0.1 < n < 0.8$ (e.g. [22]). The physical interpretation of (4.1) is that local viscoelastic dissipation in the vicinity of the crack tip sets the fracture speed. Theoretical support for the relation has been offered by Greenwood & Johnson [23] and others [13,24,25].

The work of adhesion in closing a viscoelastic crack, w_{close} , is often observed to be much less than that for peeling (e.g. [8,23]), although recent theoretical work suggests that

$$w_{\text{close}} = w_0[1 + \varphi(a_T U)]^{-1}, \quad (4.2)$$

with the same zero-speed adhesion work w_0 and empirical function φ as in the peeling relation (4.1) (e.g. [26]). However, it is also observed that contamination of the surfaces by dust particles (or roughening) can significantly reduce w_0 [18].

As a parallel to these semi-empirical models, we take

$$w_{\text{open}} = w_+ \left(1 + \frac{U^n}{U_F^n}\right) \quad \text{and} \quad w_{\text{close}} = \frac{w_-}{1 + U^n/U_F^n}, \quad (4.3)$$

where U_F is a characteristic speed. Thus, for the ruck, we make the associations, $\mathcal{W}_+(U) = w_{\text{open}}$ and $\mathcal{W}_-(U) = w_{\text{close}}$, and then balance the energy release rate with the difference between the two works of adhesion (2.11)

$$\gamma_F \equiv \frac{\rho g d \mathcal{E} \sin \theta}{w_+} = \left(1 + \frac{U^n}{U_F^n}\right) - \frac{w_-/w_+}{1 + U^n/U_F^n}. \quad (4.4)$$

This may be solved for U , giving

$$U = U_F \left(\frac{1}{2} \gamma_F - 1 + \sqrt{\frac{1}{4} \gamma_F^2 + \frac{w_-}{w_+}} \right)^{1/n}. \quad (4.5)$$

Some sample ruck speeds are shown in figure 3. Importantly, the model predicts that rucks roll provided $\gamma > 1 - w_-/w_+$. That is, once the gravitational forcing exceeds a threshold set by the difference in the two static works of adhesion: $\rho g d \mathcal{E} \sin \theta > w_+ - w_-$. The ruck rolls on any slope if $w_+ = w_-$.

(b) A thermodynamic adhesion model

Dembo *et al.* [14] propose a model for adhesion of cells (see also [27,28]) in which sticking occurs through the linking of polymer chains. There are bonded and free populations of these chains on one of the surfaces, with densities per unit area denoted A and A_f . The total areal density is fixed and spatially uniform: $A + A_f = A_T$. The reaction kinetic model for the bonded density is

$$\frac{\partial A}{\partial t} = K_0[e^{-\beta\Phi}(A_T - A) - e^{(1-\beta)\Phi}A], \quad (4.6)$$

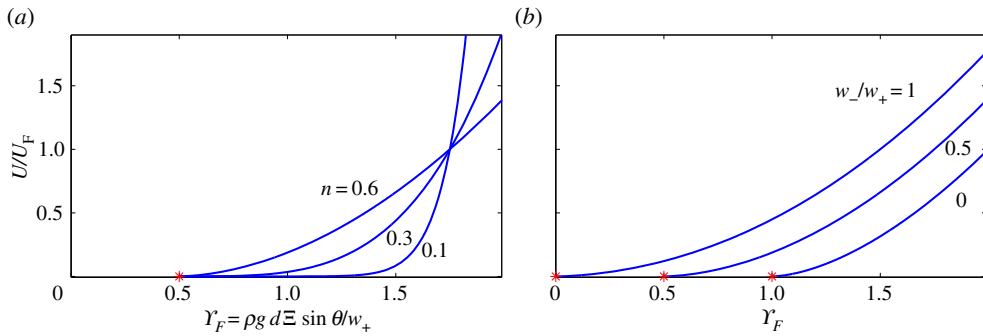


Figure 3. Dimensionless ruck speeds, U/U_F , plotted against forcing parameter Γ_F for peeling with viscoelastic cracks, with (a) $w_-/w_+ = 0.5$ and varying n , and (b) varying w_-/w_+ and $n = 0.6$. The stars mark the threshold. (Online version in colour.)

where K_0 is a rate constant and β is a constant parametrizing the different rates of attachment or detachment. The reaction rates are controlled by the ‘free energy’,

$$\Phi = \frac{\mathcal{K}\lambda^2}{2k_B T}, \quad (4.7)$$

where T is temperature, k_B is Boltzmann’s constant and the chains are assumed to behave like linear springs with constant \mathcal{K} and length λ . Dembo *et al.* discuss the significance of the sign of $1 - \beta$; here, we consider *slip bonds* with $1 > \beta$ (*catch bonds*, with $1 < \beta$, have the unusual feature that the bond strengthens as the surfaces are moved apart). Finally, Dembo *et al.* apply the spring force to the peeling surface assuming that the bonds are all perpendicular to the substrate. Hence, $\lambda \equiv Z$ and the (perpendicular) adhesive force per unit area is $\mathcal{K}\lambda A$.

Adapting this model for our ruck, we assume that the peeling layer is relatively narrow and the adhesion force is balanced primarily by bending, i.e.

$$B\lambda_{\text{ssss}} + \mathcal{K}\lambda A \approx 0.$$

For steadily rolling rucks, and in the moving frame, we then set $A_t = -UA_s$ and introduce the rescalings,

$$s = s_{\pm} + \left(\frac{B}{\mathcal{K}A_T}\right)^{1/4} \eta, \quad A = A_T a(\eta), \quad \lambda = \sqrt{\frac{k_B T}{\mathcal{K}}} g(\eta) \quad \text{and} \quad v = \frac{U}{K_0} \left(\frac{\mathcal{K}A_T}{B}\right)^{1/4}, \quad (4.8)$$

leading to the dimensionless peeling equations

$$g_{\eta\eta\eta} + ag = 0 \quad \text{and} \quad -va_{\eta} = (1-a)e^{-\beta g^2/2} - ae^{(1-\beta)g^2/2}. \quad (4.9)$$

For the peeling layer at the front of the ruck, the plate bends smoothly into ‘contact’ with the underlying plane for $s - s_+ \rightarrow \infty$. This corresponds to $g \rightarrow 0$ and $a \rightarrow \frac{1}{2}$ for $\eta \rightarrow \infty$. For $\eta \rightarrow -\infty$, g diverges algebraically into the ruck and the bond density a converges exponentially quickly to zero. The count for the number of far-field boundary conditions that must be imposed for $\eta \rightarrow \infty$ leaves us requiring a single condition for $\eta \rightarrow -\infty$, which we take to be $g_{\eta\eta} \rightarrow 0$. Thus, the solution to this peeling problem determines a value for

$$\gamma(v) \equiv g_{\eta\eta}|_{\eta \rightarrow -\infty}, \quad (4.10)$$

to which the bulk of the ruck must match. For the peeling layer at the back of the ruck, the far-field behaviours are switched around. However, the symmetry of the equations under $(\eta, v) \rightarrow (-\eta, -v)$ allow us to observe immediately that in that case $g_{\eta\eta}|_{\eta \rightarrow \infty} = \gamma(-v)$.

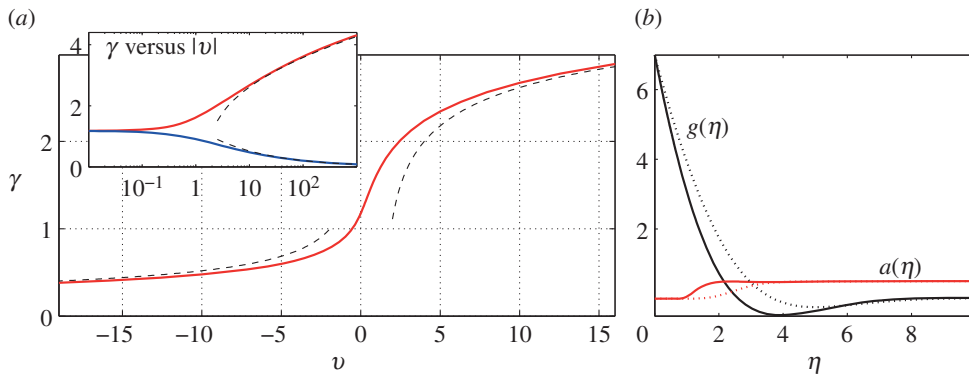


Figure 4. (a) γ against ν for $\beta = \frac{1}{2}$; in the inset the data are replotted against $|\nu|$ and using logarithmic scales (upper curve for positive, lower for negative ν). The dashed lines show limiting behaviours, $\gamma \sim 1.304(-\nu)^{-2/5}$ and $\gamma \sim \sqrt{2[\log(2^{5/4}\nu \log \nu) - 0.5772]}$. (b) Sample solutions for $g(\eta)$ and $a(\eta)$ for $\nu = 1$ (solid lines) and $\nu = -1$ (dotted lines). (Online version in colour.)

The solution for $\gamma(\nu)$ is discussed below, but first, we translate the result back to the notation of the ruck problem. We have determined

$$\mathcal{W}_{\pm}(U) = \frac{1}{2}B\kappa^2 = \frac{1}{2}k_{\text{B}}T A_T \gamma (\pm U/U_{\text{D}})^2 \quad \text{and} \quad U_{\text{D}} = K_0 \left(\frac{B}{\mathcal{K}A_T} \right)^{1/4}, \quad (4.11)$$

and so the energy constraint (2.11) is

$$\Upsilon_{\text{D}} = \frac{\rho g d \mathcal{E} \sin \theta}{(1/2)k_{\text{B}}T A_T} = \gamma \left(\frac{U}{U_{\text{D}}} \right)^2 - \gamma \left(-\frac{U}{U_{\text{D}}} \right)^2. \quad (4.12)$$

Figure 4 shows numerical computations of γ as a function of ν ; this plot is the graphical analogue of the works of adhesion in (4.3) for the viscoelastic fracture model. The curvature function increases monotonically with ν . For $\nu \rightarrow \infty$, we find $\gamma(\nu) \sim \sqrt{\log(\nu)/(1-\beta)}$; for $\nu \rightarrow -\infty$, on the other hand, the limiting behaviour is given by $\gamma(\nu) \sim \gamma_0 \beta^{-1/2} (-\nu)^{-2/5}$ with $\gamma_0 \approx 0.922$ (appendix B). Thus, for sufficiently large ruck speed, the effective adhesion energy for breaking the plate off the runway at the front of the ruck increases logarithmically, but that for sticking the plate back onto the plane becomes small. The physical reason for this behaviour is that for large ν , the effective contact points are moving relatively quickly: at the front, the bond density remains in equilibrium (with $a = \frac{1}{2}$) until the surface separation becomes sufficiently large that the exponential dissociation rate abruptly breaks all the bonds. Peeling off therefore features higher bond densities. At the back of the ruck, when the plate bends back down on the plane, the rate for bonds to reform is slow, so only a relatively small population of bonds sticks the plate back down, with the bond density recovering back to equilibrium much further uphill. Both features are evident in the large $|\nu|$ asymptotics described in appendix B.

As $\nu \rightarrow 0$, $\gamma(\nu)$ approaches a common limit from either positive or negative argument. Thus, $\Upsilon_{\text{D}} = \gamma(\nu)^2 - \gamma(-\nu)^2 \rightarrow 0$ for $\nu \rightarrow 0$. That is, there is no threshold for the onset of ruck rolling. This is illustrated in figure 5, which shows a plot of scaled ruck speed ν against the effective gravitational driving Υ_{D} , and mirrors the results for the viscoelastic fracture model in the case of the natural choice, $w_+ = w_-$. The sharp rise of the curves plotted in figure 5 results from the logarithmic dependence of $\gamma(\nu)$ for $\nu \gg 1$, which implies that the speed grows exponentially quickly at higher driving.

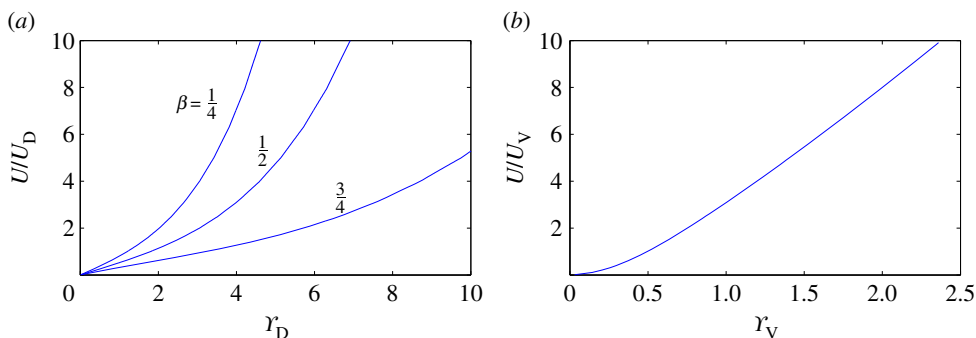


Figure 5. (a) Dimensionless ruck speed $v = U/U_D$ against gravitational driving γ_D , as determined from (4.12), for the three values of β indicated. (b) Dimensionless ruck speed $Ca = U/U_V$ against gravitational driving γ_V , as determined from (4.20). (Online version in colour.)

(c) Adhesion by a viscous film

Our third model envisions a thin viscous film of thickness δ between the undeformed beam and the underlying plane. Within the peeling regions, the fluid layer thickens as the beam bends away from the substrate and splits into two films coating the underside of the beam and the underlying plane. The peeling problem at the front of the ruck then has much in common with the so-called McEwan–Taylor problem [15].

As above, we assume that bending stresses dominate in the beam over the peeling layers, and the deflections are consequently small compared with the relevant length scales. In this case, elasto-hydrodynamic lubrication theory describes the fluid motion and beam deflection everywhere except near the meniscus where the film splits into two. The theory boils down to demanding that the fluid flux in the frame moving with the ruck is conserved.

For the peeling layer at the front, we define the ‘contact’ position, $s_+(t)$, to be the location of the meniscus (which may be treated as a single point on the scale of the whole ruck). Writing $x = s - s_+(t)$, we denote $h(x) \approx Z(s)$ as the beam deflection perpendicular to the plane. The dominant force balance for the beam is

$$Bh_{xxxx} = p, \quad (4.13)$$

where p is the pressure in the fluid film (which is approximately uniform with depth). The net fluid flux along the film must everywhere equal the flux $-U\delta$ that is provided from far upstream (that is, ahead of the ruck on the inclined plane). Upstream of the meniscus ($x > 0$), standard lubrication theory therefore requires

$$-\delta U = -hU - \frac{h^3 p_x}{12\mu}, \quad (4.14)$$

where μ is the dynamic viscosity of the fluid. Downstream of the meniscus ($x < 0$), the fluid splits into two free-surface films of uniform thickness $\frac{1}{2}\delta$, with $p = 0$ in (4.13).

For the meniscus region itself, the lubrication scalings fail and one must resort to solving the full steady Stokes equations. Following standard treatments of related problems [29,30], one can solve an appropriately rescaled ‘inner’ problem numerically, and match that solution to the ‘outer’ flow governed by (4.14). The inner solution, and therefore the match, depends on the capillary number $Ca = \mu U/\sigma$, where σ is the surface tension. We assume the film is sufficiently thin that we can ignore any effects of gravity on the fluid film.

The scalings demanded by the matched asymptotics indicate that the pressure is continuous to leading order across the meniscus region [29,30], which ensures continuity of h and its first four

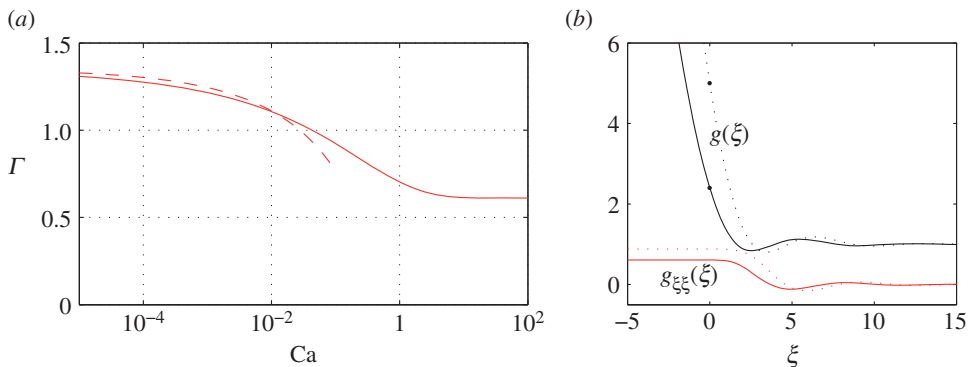


Figure 6. (a) Γ against Ca from the solution to (4.17). Solid line uses the approximation $\lambda(Ca) \approx 0.417(1 - \exp[-1.69Ca^{0.5025}])$ [32], and dashed line uses the asymptotic form $\lambda(Ca) \sim 1.34Ca^{2/3}$ for $Ca \ll 1$. (b) Sample solutions for $g(\xi)$ and $g_{\xi\xi}(\xi)$ for $\lambda = 0.417$ (solid lines) and $\lambda = 0.2$ (dotted lines). (Online version in colour.)

derivatives at $x = 0$. Moreover, the key result from the inner solution is the ratio of the fluid flux to $h(0)U$, i.e.

$$\frac{\delta}{h(0)} = \lambda(Ca), \quad (4.15)$$

where $\lambda(Ca)$ is a monotonically increasing function of Ca with limits $\lambda(Ca) \sim 1.34Ca^{2/3}$ for $Ca \ll 1$ and $\lambda(Ca) \rightarrow 0.417$ for $Ca \rightarrow \infty$ [15,30,31].

Recasting the problem in dimensionless form, we write

$$x = \left(\frac{B\delta^3}{12\mu U} \right)^{1/5} \xi \quad \text{and} \quad h(x) = \delta g(\xi), \quad (4.16)$$

and arrive at the dimensionless peeling equation

$$g_{\xi\xi\xi\xi\xi} = \frac{1-g}{g^3}, \quad (4.17)$$

for $\xi > 0$. The requirement $g \rightarrow 1$ for $\xi \rightarrow \infty$ imposes two boundary conditions, leaving three conditions to apply at $\xi = 0$. One of these is the dimensionless version of (4.15), $g(0) = 1/\lambda(Ca)$, and another is the pressure continuity condition $g_{\xi\xi\xi\xi}(0) = 0$. We may therefore additionally impose $g_{\xi\xi\xi}(0) = 0$, which furnishes a quadratic solution for g in $\xi < 0$. The far-field curvature is thus determined as

$$\Gamma(Ca) \equiv g_{\xi\xi}|_{\xi \rightarrow -\infty} = g_{\xi\xi}(0). \quad (4.18)$$

Figure 6 shows the numerical computations of $\Gamma(Ca)$, making use of fitted and asymptotic forms for $\lambda(Ca)$ stated above.

For the peeling region at the back of the ruck, we take $x = s - s_-(t)$ and follow the same analysis to arrive at the peeling equation (4.17) but now to be solved for $\xi < 0$. Imposing $g \rightarrow 1$ as $\xi \rightarrow \infty$ now furnishes three boundary conditions, limiting us to two further ones at $\xi = 0$, namely $g(0) = 1/\lambda(Ca)$ and $g_{\xi\xi\xi\xi}(0) = 0$. The solution in $\xi > 0$ is therefore cubic. In order to match with the main ruck solution, this demands that the limiting curvature, $\kappa_- = 0$. No details of the matched asymptotics are needed in this case; one only needs the guarantee that the asymptotic scheme is successful. This does indeed appear so for low enough Ca ; at higher capillary number there appear to be some hidden issues [33].

The preceding results translate to the dimensional works of adhesion

$$\mathcal{W}_+(U) = \frac{1}{2} \delta^{-2/5} B^{1/5} (12\mu U)^{4/5} \Gamma \left(\frac{\mu U}{\sigma} \right)^2 \quad \text{and} \quad \mathcal{W}_- = 0. \quad (4.19)$$

Thus, the energy constraint (2.11) becomes

$$\Upsilon_V \equiv \frac{\rho g d \mathcal{E} \sin \theta}{(1/2)(12)^{4/5} \sigma (B/\sigma \delta^2)^{1/5}} = \left(\frac{U}{U_V} \right)^{4/5} \Gamma \left(\frac{U}{U_V} \right)^2 \quad \text{and} \quad U_V = \frac{\sigma}{\mu}. \quad (4.20)$$

Figure 5 shows the relationship between U and the dimensionless gravitational driving Υ_V . Once again, there is no threshold for rolling; even though there is no adhesion at the back of the ruck ($\mathcal{W}_- = 0$), the work needed to peel the ruck off the plane at the front vanishes with the ruck speed.

5. Ruck experiments

Our experiments are summarized in figure 7. We placed a PVC sheet of thickness 3 mm on a 45° incline, securing each end with clamps to prevent any sliding. For most of the experiments, the runway was covered by 60-grit sandpaper to provide a controlled degree of surface roughness. A ruck was created by moving the bottom of the sheet a given distance \mathcal{E} up the runway, and then working the resulting buckle up to the top of the runway, where it was released. The buckle subsequently converged to a rolling ruck whose speed we estimated either by timing when the ruck passed fixed positions on the runway, or from linear fits to the central position of the ruck extracted from video frames. The video data indicated that the rucks reached a fairly steady rolling speed, although there were systematic variations that we ascribed to inhomogeneities in the rubber sheet (rucks ‘wobbled’ at similar positions in repeated experiments, figure 7c).

The measured ruck speeds are plotted against foreshortening \mathcal{E} in figure 7a. Qualitatively, the results resonate with our theoretical predictions in figures 3 and 5, and also with the results presented by Kolinski *et al.* (their fig. 4b). By contrast, bulk dissipation suggests a steep rise of the ruck speed with small \mathcal{E} (§3), which is not consistent with the experimental data. Thus, a local mechanism within the peeling regions seems more likely than bulk dissipation in controlling the rolling speed.

Two difficulties arose in performing repeatable experiments. First, after the sheet was left in an undeformed state for periods of order a day, the speeds of the first few rucks to be rolled were observed to increase systematically with the order in which they were released (figure 7b). We interpreted this ‘work-in’ effect to result from the relaxation character of the rubber material, much as is known in other contexts. Second, when performing experiments on different days, ruck speeds could differ even for the same foreshortening \mathcal{E} (cf. the spread of speeds for $\mathcal{E} = 17$ cm in figure 7a, which correspond to three different experimental sequences). This effect could have a number of origins: the temperature was not controlled in the laboratory and varied by a few degrees day to day; each time the sheet was clamped, an unknown amount of tension could have been introduced; whenever a ruck was rolled, the sandpaper gradually scratched the underside of the rubber sheet; the rubber clearly possessed a memory of its state of deformation, with imprints from long-lived wrinkles or folds persisting for long times after being straightened, and affecting subsequent ruck rolls. Rather than chase down the precise reason for this day-to-day variation, we elected to accept its presence and mostly focus on sequences of experiments run on the same day and with the same clamping, which showed a fair degree of reproducibility once the sheet had been worked-in (figure 7c).

A surprise in our experiments was that ruck speeds varied little when we changed the type of sandpaper covering the runway, replaced it with a smooth plastic sheet, or removed it entirely to leave a sticky wooden surface (the sandpaper was glued down, and some of the adhesive was left behind after its removal) (figure 7d). This observation casts doubt on any interpretation that relies on the detailed surface properties, as in the kinetic and viscous peeling models in §4b,c. The viscoelastic fracture model therefore appears to be the most plausible explanation.

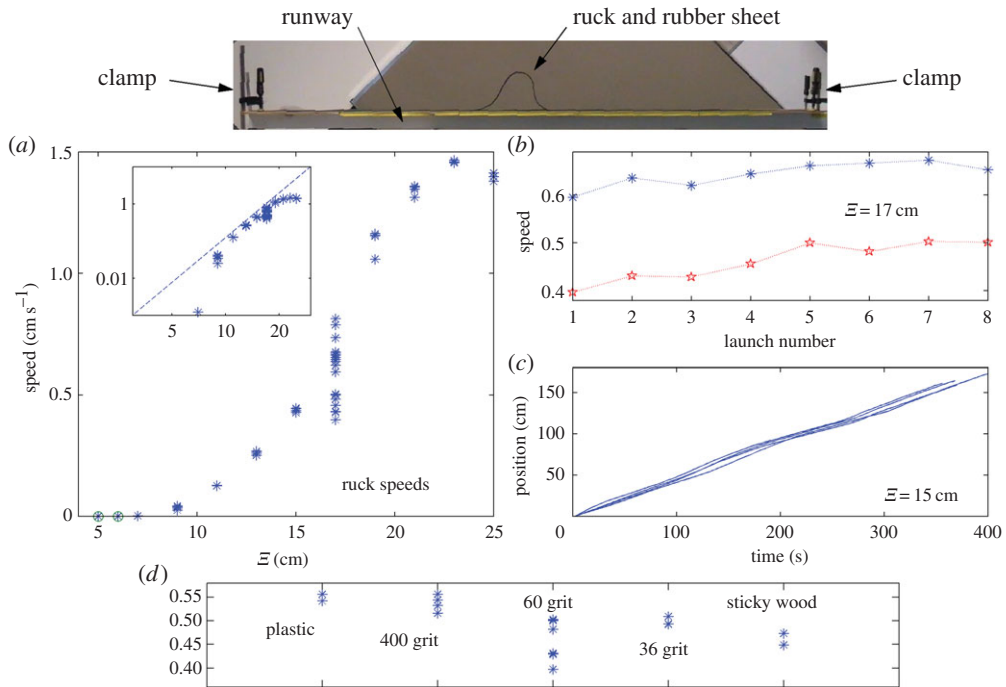


Figure 7. The top photograph shows a ruck in the clamped rubber sheet on the 45° runway (a wooden board reinforced with a metal frame). (a) Measured ruck speeds against foreshortening length Ξ ; the data are plotted logarithmically in the inset; the dashed line shows the dependence Ξ^4 . (b) How the speed varied with the launch number of the ruck for $\Xi = 17$ cm during two different sequences of experiments on different days and clampings. (c) The central position of four rucks during one sequence of experiments with $\Xi = 15$ cm; in this case, several rucks with varying Ξ have already been run down the incline (so the sheet has been ‘worked-in’). The bottom panel (d) shows how ruck speeds with $\Xi = 17$ cm varied between sequences of experiments on the same day and clamping but different coverings on the wooden plane. (Online version in colour.)

That model still requires some surface adhesive energy, but the crucial dissipation occurs within the rubber and is controlled by its internal material properties rather than those of the interface. To temper this conclusion, we observed that the situation was quite different in some qualitative experiments that were performed with a sheet of PDMS rubber: for this material, ruck speeds varied significantly when one changed the underlying surface (the material is also discernibly tackier than the PVC).

In appendix A, we estimate physical constants in each of our three models. There is a great deal of uncertainty so we cannot clearly rule out any of the models in comparison to our experiments or to the earlier results of Kolinski *et al.* It is entirely possible that different mechanisms dominate in different circumstances, depending on the specific material and substrate.

Finally, we mention some additional experimental observations of ruck interactions. Because ruck speed depends on amplitude, one can launch rucks of differing size into collisions to explore how they interact. We observe (figure 8) that to trigger a collision, the larger ruck must lie uphill, as expected given the predicted relationships between ruck size and speed. When this ruck reaches the back of the ruck in front, it is unable to lift the sheet off the runway between the two structures. Instead, it becomes obstructed and slows down, and also drives the preceding ruck forwards to accelerate it, generating a steadily propagating double-ruck state. The detailed mechanism by which the ruck interaction takes place is not clear, as the sheet is in contact with the runway over a narrow, but finite section between the two rucks. Our peeling models say nothing about such interaction. However, the overall effect is that the ruck at the front controls the speed of the bound pair that forms from the collision.

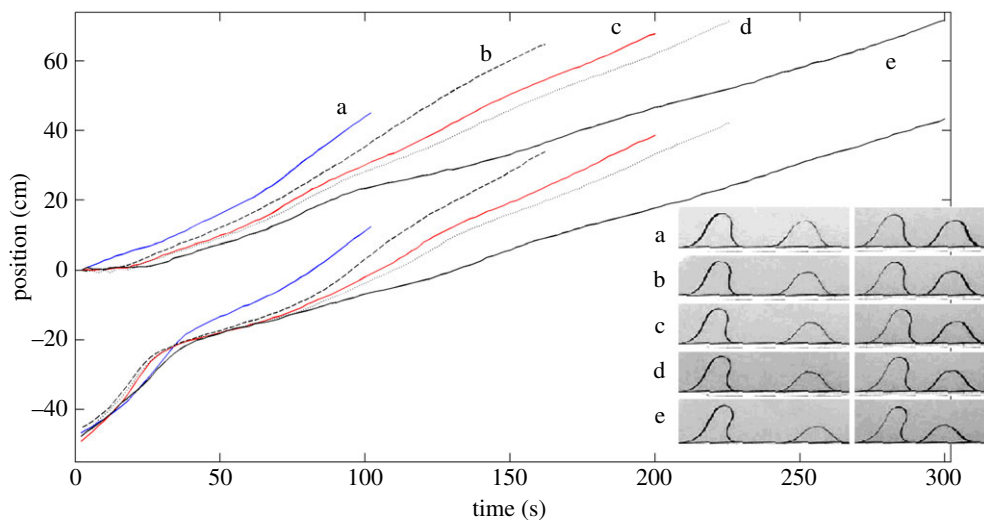


Figure 8. Experiments in which a foreshortening of about 30 cm was divided up into two rucks of unequal size. Five cases are shown, with the ruck at the rear being gradually increased in size at the expense of the ruck at the front. Shown are the central positions of the two rucks, together with snapshots of the profiles at the beginning and end of the experiments. (Online version in colour.)

6. Conclusion

We have explored theoretically the dynamics of rucks in an elastic sheet rolling down an inclined plane, focusing on what sets the rolling speed. In particular, we have reconsidered the two global dissipative mechanisms for controlling the steady rolling speed mentioned by Kolinski *et al.* [1], air drag and bulk viscoelasticity, and we have studied three possible processes that might control the speed through narrow peeling layers at the fore and aft of the ruck. The peeling models are based on viscoelastic crack propagation, a kinetic model for the breakage of bonds spanning the contacting surfaces, and an intervening adhesive viscous film.

The key conclusion of our analysis is that the ruck speed is set by the velocity dependence of either the global dissipation or the local peeling dynamics, as quantified by the integral expressions (2.9) or (3.1). With that in mind, we closed by comparing the predictions with experiments. The experimental results lend support to the conclusion that local peeling dynamics control the speed of the ruck. However, all of the peeling models provide qualitative agreement with the experiments, and given the large uncertainty in parameters, we are unable to clearly rule out any of the mechanisms.

A qualitative problem with our theory is the threshold for rolling observed in both the experiments by Kolinski *et al.* and our own (rucks with $\mathcal{E} < 7$ cm appeared to decelerate to rest on the 45° incline). No such threshold emerges in either the thermodynamic or viscous adhesive models, and if the static energies of adhesion for breaking and making contacts are taken to be the same ($w_+ = w_-$) nor is there a threshold with the viscoelastic fracture model. To compound matters, Kolinski *et al.* [1] report a different threshold for the onset and cessation of rolling, in a manner reminiscent of the discrepancy between dynamic and static friction, or capillary hysteresis (e.g. [34]).

The absence of a threshold in our theory reflects the fact that although the front and back peeling conditions are velocity dependent, they always become identical in the limit of vanishing velocity. Any kinetic or viscous theory inherently relies upon motion to generate fore-aft asymmetry and therefore cannot generate a threshold. This suggests that some other physical process must be responsible for arresting motion and effecting the necessary balance in (2.9). One can manufacture the threshold in the fracture model by simply adopting a difference in the fore-aft works of adhesion, but this has yet to be derived from any theoretical argument. Similarly,

in the thermodynamic model one can assume that the bonds are permanently broken once they detach, in which case the lack of adhesion at the back provides a threshold. Alternatively, the threshold may be associated with the material's memory: long-lived deformation alters the neutral stress state over time, which might conceivably arrest motion if relaxation is quicker than rolling.

Acknowledgements. We thank Jerome Neufeld and Dominic Vella for discussions.

Funding statement. R.V.C. thanks the EPSRC for support under the platform grant no. EP/L020564/1.

Appendix A. Physical parameter estimates

Here, we summarize estimates of the physical constants in each of the peeling models. The exercise is fraught with uncertainty because of a lack of information regarding the relevant material properties.

For our experiments, we used a 3 mm thick, 7.5 cm wide PVC sheet of density 1.63 g cm^{-3} placed on a 45° incline. The PVC sheet was cut from a strip of commercially available rubber wall protection ('Shur-Trim wall cove base'). From simple tests based on the gravitational deflection of a section of the rubber clamped horizontally at one end, we estimated that $L_b = (B/\rho g d)^{1/3} = 9 \text{ cm}$ or $B \approx 0.035 \text{ kg m}^2 \text{ s}^{-2}$. For typical values of $\mathcal{E} = 10 \text{ cm}$, and $U = 1 \text{ cm s}^{-1}$, we estimate the gravitational forcing $\rho g d \mathcal{E} \approx 5 \text{ J m}^{-2}$. By looking at decaying oscillations of the beam we also estimated $C = 3 \times 10^{-4} \text{ J s}$ for the bulk viscoelastic parameter of §3.

For Kolinski *et al.*'s [1] experiments, we take $\rho = 10^3 \text{ kg m}^{-3}$, $d = 1 \text{ mm}$, $\nu = 0.5$, $E = 10^6 \text{ Pa}$, $B = 10^{-4} \text{ kg m}^2 \text{ s}^{-2}$ and typical values $\mathcal{E} = 1 \text{ cm}$, $\sin \theta = O(1)$ and $U = 1 \text{ m s}^{-1}$. Hence, $\rho g d \mathcal{E} \approx 0.1 \text{ J m}^{-2}$.

For many surfaces, the work of adhesion w_0 (or w_\pm) is quoted to be of the order of 0.1 J m^{-2} . Estimates of the parameters (n, U_F) in the fit (4.3) are more varied: data for a PDMS surface in contact with glass or acrylic suggest a range from $(0.4, 10^{-6} \text{ m s}^{-1})$ to $(0.12, 10^{-9} \text{ m s}^{-1})$ [18,22]. Data from Gent [35], Maugis & Barquins [21] and Shull [13] indicate that $(n, U_F) \sim (0.25, 10^{-12} \text{ m s}^{-1})$ for a styrene butadiene rubber, $(0.6, 10^{-6} \text{ m s}^{-1})$ for polyurethane, and $(0.6, 10^{-8} \text{ m s}^{-1})$ for PNBA, respectively. Fig. 4 of Kendall [8] suggests a slightly higher work of adhesion for peeling, $w_+ = 1 \text{ J m}^{-2}$, $w_- = 0.1 \text{ J m}^{-2}$, and estimates of (n, U_F) that could be as large as $(0.6, 10^{-4} \text{ m s}^{-1})$, for rubber in contact with glass.

For the thermodynamic model, we estimate $A_T = 10^{16} \text{ m}^{-2}$, $k_B T = O(10^{-21}) \text{ J}$, $\mathcal{K} = 1 \text{ kg s}^{-2}$ and $K_0 = 10^{-10}$ to 0.1 s^{-1} based on values given by Ghatak *et al.* [17]. The value of the reaction rate K_0 is particularly uncertain.

For fluid adhesion, we consider a film of water with surface tension $\sigma = 0.1 \text{ N m}^{-1}$, dynamic viscosity of $\mu = 10^{-3} \text{ Pa s}$, and take the film to have a thickness of $\delta = 10^{-9}$ to 10^{-6} m .

One can use these parameter estimates to manufacture theoretical ruck speeds to compare with the observations. Unfortunately, in none of the cases can one convincingly rule out a particular model.

Appendix B. Asymptotics of the thermodynamic peeling model

Here we consider the asymptotic limits of the peeling equations (4.9) for $|v| \gg 1$, seeking to determine the matching value of the curvature $\gamma(v) = g_{\eta\eta}|_{\eta \rightarrow -\infty}$. Sample numerical solutions for comparison are shown in figure 9, and the results of this analysis are compared with the full numerical solutions in figure 4.

(a) $v \gg 1$

For large positive v , $a(\eta)$ remains constant over most of the domain, but jumps from $\frac{1}{2}$ to 0 over a narrow boundary layer in which g is relatively large so that the final exponential term in (4.9) balances va_η (figure 9a). For the analysis below, we located the boundary layer at $\eta = 0$; the numerical solution in figure 9a has a different choice of origin.

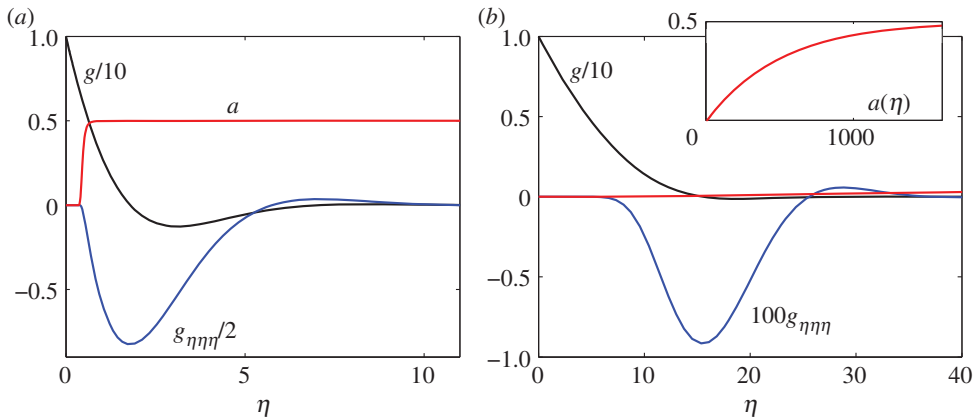


Figure 9. Solution of the peeling equations (4.9) for (a) $\nu = 10^3$ and (b) $\nu = -10^3$. Shown are g and $g_{\eta\eta\eta}$ (both scaled as indicated) and a . The inset of (b) shows the relaxation of a towards $\frac{1}{2}$ over a longer domain. (Online version in colour.)

To the right of the boundary layer, $a \sim \frac{1}{2}$ and $g_{\eta\eta\eta} + \frac{1}{2}g \sim 0$. Hence,

$$g \sim \frac{g_0 e^{-m\eta} \sin(m\eta - \varphi)}{\sin(-\varphi)}, \quad m = 2^{-3/4}, \tag{B1}$$

where $g_0 = g(0)$ and φ is an unknown phase. To the left of the boundary layer, $g_{\eta\eta\eta} \sim 0$, which implies a quadratic solution for $g(\eta)$ given that $g_{\eta\eta\eta} \rightarrow 0$ as $\eta \rightarrow -\infty$. The boundary layer is sufficiently narrow that g , g_η , $g_{\eta\eta}$ and $g_{\eta\eta\eta}$ remain continuous across it to leading order (see below). We therefore require $g_{\eta\eta\eta}(0) = 0$ or $\varphi = \frac{1}{4}\pi$, and

$$g \sim g_0[1 - 2m\eta + m^2\eta^2], \tag{B2}$$

to the left of the boundary layer.

Within the boundary layer, we set $\eta = \delta\tilde{\eta}$ and $\tilde{\eta}_* = [2m(1 - \beta)g_0^2\delta]^{-1}$, where $\delta = \nu e^{-(1-\beta)g_0^2/2}$ (anticipating $\delta = \mathcal{O}(1/\ln \nu) \ll 1$, $\tilde{\eta}_* = \mathcal{O}(1)$, as verified below), to furnish the rescaled problem,

$$g_{\tilde{\eta}\tilde{\eta}\tilde{\eta}} \sim -\delta^4 g_0 a \quad \text{and} \quad a_{\tilde{\eta}} \sim a e^{-\tilde{\eta}/\tilde{\eta}_*}, \tag{B3}$$

subject to the matching conditions, $a \rightarrow 0$ as $\tilde{\eta} \rightarrow -\infty$, $a \rightarrow \frac{1}{2}$ as $\tilde{\eta} \rightarrow \infty$ and $g_{\tilde{\eta}\tilde{\eta}\tilde{\eta}} \rightarrow 0$ as $\tilde{\eta} \rightarrow -\infty$, $g_{\tilde{\eta}\tilde{\eta}\tilde{\eta}} \rightarrow -\frac{1}{2}\delta^4 g_0$ as $\tilde{\eta} \rightarrow \infty$; the scaling $g_{\tilde{\eta}\tilde{\eta}\tilde{\eta}} = \mathcal{O}(\delta^4)$ justifies the continuity of the lower derivatives across the boundary layer.

The solution for a which matches correctly to either side is

$$a \sim \frac{1}{2} \exp(-\tilde{\eta} e^{-\tilde{\eta}/\tilde{\eta}_*}). \tag{B4}$$

Integrating the first equation in (B3) therefore gives

$$g_{\tilde{\eta}\tilde{\eta}\tilde{\eta}}(\tilde{\eta}) \sim -\frac{1}{2}\delta^4 g_0 E_1[\tilde{\eta} e^{-\tilde{\eta}/\tilde{\eta}_*}], \tag{B5}$$

where $E_1[x] = \int_x^\infty e^{-u}/u \, du$. This exponential integral has the asymptotic form $E_1[x] \sim -\gamma_E - \ln x + \mathcal{O}(x)$ for small x , where $\gamma_E \approx 0.5772$ is Euler's constant. Matching for large $\tilde{\eta}$ then requires

$$-\frac{1}{2}g_0\tilde{\eta} \sim \frac{1}{2}g_0[\gamma_E + \ln \tilde{\eta}_*] - \frac{1}{2}g_0\tilde{\eta}, \tag{B6}$$

and so

$$\tilde{\eta}_* = \frac{e^{(1-\beta)g_0^2/2}}{2m(1 - \beta)g_0^2\nu} = e^{-\gamma_E}, \tag{B7}$$

which implicitly determines g_0 in terms of v . Expanding in $\log v$, we finally obtain

$$\gamma(v) \sim \frac{g_0}{2^{1/2}} \sim \sqrt{\frac{\log(v \log v) + (5/4) \log 2 - \gamma_E}{1 - \beta}}. \quad (\text{B } 8)$$

(b) $-v \gg 1$

For large negative v , $g(\eta)$ remains close to zero whilst $a(\eta)$ decays exponentially from $\frac{1}{2}$ on the right towards 0 over a distance of length $O(|v|)$: $g \sim 0$ and $a \sim \frac{1}{2}(1 - e^{-2\eta/|v|})$, on selecting the origin of η as the location where $a \rightarrow 0$ according to this outer solution. A boundary layer then arises around $\eta = 0$ of width $O(|v|^{1/5})$, where $a = O(|v|^{-4/5})$. See figure 9b. Rescaling according to

$$\eta = |v|^{1/5} \zeta, \quad g = \beta^{-1/2} \tilde{g}(\zeta) \quad \text{and} \quad a = |v|^{-4/5} \tilde{a}(\zeta), \quad (\text{B } 9)$$

we then recover the (parameterless) problem,

$$\tilde{g}_{\zeta\zeta\zeta\zeta} + \tilde{a}\tilde{g} = 0 \quad \text{and} \quad \tilde{a}_{\zeta} = e^{-\tilde{g}^2/2}. \quad (\text{B } 10)$$

Numerically solving this problem using boundary conditions equivalent to those imposed on (4.9) indicates that $\gamma(v) \sim 0.922\beta^{-1/2}(-v)^{-2/5}$.

References

- Kolinski JM, Aussillous P, Mahadevan L. 2009 Shape and motion of a ruck in a rug. *Phys. Rev. Lett.* **103**, 174302. (doi:10.1103/PhysRevLett.103.174302)
- Vella D, Boudaoud A, Adda-Bedia M. 2009 Statics and inertial dynamics of a ruck in a rug. *Phys. Rev. Lett.* **103**, 174301. (doi:10.1103/PhysRevLett.103.174301)
- Gittus JH. 1975 Interfacial dislocations in frictional sliding and interfacial creep: the theory of interfacions. *Philos. Mag.* **31**, 317–329. (doi:10.1080/14786437508228935)
- Heaton TH. 1990 Evidence for and implications of self-healing pulses of slip in earthquake rupture. *Phys. Earth Planet. Inter.* **64**, 1–20. (doi:10.1016/0031-9201(90)90002-F)
- Kendall K. 1976 Preparation and properties of rubber dislocations. *Nature* **261**, 35–36. (doi:10.1038/261035a0)
- Briggs GAD, Briscoe BJ. 1978 How rubber grips and slips Schallamach waves and the friction of elastomers. *Philos. Mag. A* **38**, 387–399. (doi:10.1080/01418617808239243)
- Charras GT, Coughlin M, Mitchison TJ, Mahadevan L. 2008 Life and times of a cellular bleb. *Biophys. J.* **94**, 1836–1853. (doi:10.1529/biophysj.107.113605)
- Kendall K. 1975 Rolling friction and adhesion between smooth solids. *Wear* **33**, 351–358. (doi:10.1016/0043-1648(75)90288-4)
- Roberts AD, Thomas AG. 1975 The adhesion and friction of smooth rubber surfaces. *Wear* **33**, 45–64. (doi:10.1016/0043-1648(75)90223-9)
- Lister JR, Peng GG, Neufeld JA. 2013 Viscous control of peeling an elastic sheet by bending and pulling. *Phys. Rev. Lett.* **111**, 154501. (doi:10.1103/PhysRevLett.111.154501)
- Hewitt IJ, Balmforth NJ, De Bruyn JR. In press. Elastic-plated gravity currents. *Eur. J. Appl. Math.* (doi:10.1017/S0956792514000291)
- Maugis D. 2001 Adhesion of solids: mechanical aspects. *Modern tribology handbook*, vol. 1. Boca Raton, FL: CRC Press.
- Shull KR. 2002 Contact mechanics and the adhesion of soft solids. *Mater. Sci. Eng.* **36**, 1–45. (doi:10.1016/S0927-796X(01)00039-0)
- Dembo M, Torney DC, Saxman K, Hammer D. 1988 The reaction-limited kinetics of membrane-to-surface adhesion and detachment. *Proc. R. Soc. Lond. B* **234**, 55–83. (doi:10.1098/rspb.1988.0038)
- McEwan AD, Taylor GI. 1966 The peeling of a flexible strip attached by a viscous adhesive. *J. Fluid Mech.* **26**, 1–15. (doi:10.1017/S0022112066001058)
- Kendall K. 1973 Peel adhesion of solid films—the surface and bulk effects. *J. Adhesion* **5**, 179–202. (doi:10.1080/00218467308075019)
- Ghatak A, Vorvolakos K, She H, Malotky DL, Chaudhury MK. 2000 Interfacial rate processes in adhesion and friction. *J. Phys. Chem. B* **104**, 4018–4030. (doi:10.1021/jp9942973)

18. Lorenz B, Krick BA, Mulakaluri N, Smolyakova M, Dieluweit S, Sawyer WG, Persson BNJ. 2013 Adhesion: role of bulk viscoelasticity and surface roughness. *J. Phys. Condens. Matter* **25**, 225004. (doi:10.1088/0953-8984/25/22/225004)
19. Wang CY. 1986 A critical review of the heavy elastica. *Int. J. Mech. Sci.* **28**, 549–559. (doi:10.1016/0020-7403(86)90052-4)
20. Flaherty JE, Keller JB. 1973 Contact problems involving a buckled elastica. *SIAM J. Appl. Math.* **24**, 215–225. (doi:10.1137/0124022)
21. Maugis D, Barquins M. 1978 Fracture mechanics and the adherence of viscoelastic bodies. *J. Phys. D* **11**, 1989. (doi:10.1088/0022-3727/11/14/011)
22. Waters JF, Guduru PR. 2009 Mode-mixity-dependent adhesive contact of a sphere on a plane surface. *Proc. R. Soc. A* **466**, 1303–1325. (doi:10.1098/rspa.2009.0461)
23. Greenwood JA, Johnson KL. 1981 The mechanics of adhesion of viscoelastic solids. *Philos. Mag. A* **43**, 697–711. (doi:10.1080/01418618108240402)
24. Persson BNJ, Albohr O, Heinrich G, Ueba H. 2005 Crack propagation in rubber-like materials. *J. Phys. Condens. Matter* **17**, R1071. (doi:10.1088/0953-8984/17/44/R01)
25. Persson BNJ, Brener EA. 2005 Crack propagation in viscoelastic solids. *Phys. Rev. E* **71**, 036123. (doi:10.1103/PhysRevE.71.036123)
26. Greenwood JA. 2004 The theory of viscoelastic crack propagation and healing. *J. Phys. D* **37**, 2557. (doi:10.1088/0022-3727/37/18/011)
27. Hodges SR, Jensen OE. 2002 Spreading and peeling dynamics in a model of cell adhesion. *J. Fluid Mech.* **460**, 381–409. (doi:10.1017/S0022112002008340)
28. Mani M, Gopinath A, Mahadevan L. 2012 How things get stuck: kinetics, elastohydrodynamics, and soft adhesion. *Phys. Rev. Lett.* **108**, 226104. (doi:10.1103/PhysRevLett.108.226104)
29. Ruschak KJ. 1982 Boundary conditions at a liquid/air interface in lubrication flows. *J. Fluid Mech.* **119**, 107–120. (doi:10.1017/S0022112082001281)
30. Jensen OE, Horsburgh MK, Halpern D, Gaver III, DP. 2002 The steady propagation of a bubble in a flexible-walled channel: asymptotic and computational models. *Phys. Fluids* **14**, 443–457. (doi:10.1063/1.1432694)
31. Bretherton FP. 1961 The motion of long bubbles in tubes. *J. Fluid Mech.* **10**, 166–188. (doi:10.1017/S0022112061000160)
32. Halpern D, Gaver III, DP. 1994 Boundary element analysis of the time-dependent motion of a semi-infinite bubble in a channel. *J. Comput. Phys.* **115**, 366–375. (doi:10.1006/jcph.1994.1202)
33. Taroni M, Breward CJW, Howell PD, Oliver JM. 2012 Boundary conditions for free surface inlet and outlet problems. *J. Fluid Mech.* **708**, 100–110. (doi:10.1017/jfm.2012.275)
34. Bonn D, Eggers J, Indekeu J, Meunier J, Rolley E. 2009 Wetting and spreading. *Rev. Mod. Phys.* **81**, 739. (doi:10.1103/RevModPhys.81.739)
35. Gent AN. 1996 Adhesion and strength of viscoelastic solids. is there a relationship between adhesion and bulk properties? *Langmuir* **12**, 4492–4496. (doi:10.1021/la950887q)